Quaternary Science Reviews 307 (2023) 108056

Contents lists available at ScienceDirect

Quaternary Science Reviews

journal homepage: www.elsevier.com/locate/quascirev

Atlantic ITCZ variability during the Holocene based on high-resolution speleothem isotope records from northern Venezuela

N. Melissa M. Medina [a, *], Francisco W. Cruz [a], Amos Winter [b, c], Haiwei Zhang [d], Angela Ampuero [a], Mathias Vuille [e], Víctor C. Mayta [f], Marília C. Campos [a], Veronica Marcela Ramirez [a], Giselle Utida [a], Andres Camilo Zúñiga [g], Hai Cheng [d, h]

[a] Institute of Geosciences, University of São Paulo, São Paulo, 05508-080, Brazil
[b] Department of Earth and Environmental Systems, Indiana State University, Terre Haute, 47809, IN, USA
[c] Department of Marine Sciences, University of Puerto Rico, Mayaguez, 00680, Puerto Rico, USA
[d] Institute of Global Environmental Change, Xi'an Jiaotong University, Xi'an, 710049, China
[e] Department of Atmospheric and Environmental Sciences, University at Albany, Albany, NY, 12222, USA
[f] Department of Atmospheric and Oceanic Sciences, University of WisconsineMadison, Madison, WI, USA
[g] Departamento de Ciencias Biologicas, Universidad de Los Andes, Bogota D.C., Colombia
[h] State Key Laboratory of Loess and Quaternary Geology, Institute of Earth Environment, Chinese Academy of Sciences, Xi'an, 710061, China

a r t i c l e i n f o

Article history:
Received 24 September 2022
Received in revised form
8 February 2023
Accepted 18 March 2023
Available online xxx

Handling Editor: Yan Zhao

Keywords:
Intertropical convergence zone
Holocene
Venezuela
Speleothems
Paleoclimate
Stable isotopes
South America
Cariaco basin
Caribbean
Bond cycles
NADW
AMO

a b s t r a c t

Few high-resolution paleoclimate proxy records exist in the region located under the direct influence of the Intertropical Convergence Zone (ITCZ) in South America and most of them were retrieved from the Cariaco Basin off the coast of Venezuela. Here we present new $\delta^{18}O$ and $\delta^{13}C$ records of Venezuelan speleothems collected in caves adjacent to Cariaco, covering the mid- and late-Holocene. We document previously undetected secular-to multidecadal-scale climate variability in the core region of the ITCZ, which is compared to other high-resolution records from the North Atlantic, Caribbean and tropical South America. Over the mid-Holocene our record exhibits broad swings between periods of reduced (8.3e8.0, 6.5e5.0, 4.1e3.6 ka BP) and increased (8.5, 8.0e6.5, 4.9e4.2 ka BP) rainfall. In particular, between 5.5 and 5.0 ka BP, increases in polar and subpolar North Atlantic ice rafted debris and a reduction in North Atlantic Deep Water (NADW) formation might have contributed to the southward displacement of the North Atlantic Subtropical High (NASH) and the ITCZ, which led to severe dry conditions in north central Venezuela and an enhancement of the South American Monsoon System (SAMS). During the late-Holocene, contrary to data from Cariaco reported in previous studies, our results point to drier conditions during the Medieval Climate Anomaly (MCA, 900e1100 CE), which were further amplified during positive Atlantic Multidecadal Oscillation (AMO) phases. Wet conditions, however, prevailed during the first part of the Little Ice Age (LIA, 1400e1500 CE). No speleothem deposition occurred during the main LIA period, which might be related to drier conditions in response to a southward displacement of the ITCZ that led to major moisture convergence over the SASM domain. Our new records from Venezuela provide a reliable proxy for ITCZ behavior over the Atlantic e South America domain and document past dynamics in relation to other climate systems (NASH and SAMS), while providing new evidence of ITCZ e North Atlantic teleconnections during the Holocene.

1. Introduction

The meridional migration of the western Atlantic Intertropical Convergence Zone (ITCZ) towards the differentially warmer hemisphere, exerts a strong control of the annual cycle of precipitation in northern South America and southeastern Caribbean regions (Poveda et al., 2006; Martinez et al., 2019). One of the primary areas that has been used to study the ITCZ on longer time scales is the Cariaco Basin (located in the northern continental shelf of Venezuela, northern South America) (Peterson et al., 2000; Haug et al., 2001), where several proxy data sets have been analyzed, some extending back in time to 600 thousand years before present

* Corresponding author.
E-mail address: melissam@usp.br (N.M.M. Medina).

https://doi.org/10.1016/j.quascirev.2023.108056
0277-3791/

(ka BP) (Peterson et al., 2000; Gibson and Peterson, 2014). The temporal resolution for some of these proxies reaches ca. ~4e5 years for the last 14 ka BP (Haug et al., 2001), due to local high sedimentation rates (0.3 to >1 mm/year) under virtually anoxic conditions.

Several studies have analyzed various proxies in marine sediment cores from the Cariaco Basin: Mo (ventilation, Yarincik et al., 2000; Gibson and Peterson, 2014); gray-scale and total reflectance (relative input of marine and terrigenous sediments, Hughen et al., 1996; Hughen et al., 2000; Deplazes et al., 2013); alkenone concentration (surface productivity, Herbert and Schuffert, 2000; Goni et al., 2004); Mg/Ca (sea surface temperatures-SSTs, Lea et al., 2003; Wurtzel et al., 2013); Ti (continental runoff, Haug et al., 2001; Peterson & Haug, 2006). Most of these studies indicate rapid reorganization of ocean-atmosphere teleconnections in the past during glacial-interglacial transitions and millennial-scale events such as the Dansgaard/Oeschger cycles (DO) and Heinrich events. During Heinrich events, rapid iceberg discharge reduced North Atlantic Deep Water (NADW) formation, triggering the slowdown of the Atlantic Meridional Overturning Circulation (AMOC). These events have been associated with a strengthening of the northeastern trade winds and a southern ITCZ position relative to Cariaco (Lea et al., 2003; Deplazes et al., 2013; Bohm et al., 2015; Mulitza et al., 2017). Paleoclimate records under the influence of the South American Monsoon System (SAMS) support this connection over millennial and also centennial scales by showing precipitation increases during periods of a more southern ITCZ location, which acts as a moisture conduit for monsoon precipitation (Bird et al., 2011; Vuille et al., 2012; Stríkis et al., 2015).

For the Holocene, the hydroclimate changes derived from the numerous proxy records from Cariaco are less consistent. Still, the Ti concentration in sediments (Haug et al., 2001) has been interpreted in several data and modeling studies as providing unequivocal evidence for the southward displacement of the western Atlantic ITCZ from the mid-to the late-Holocene, following the gradual decrease in local insolation (Dykoski et al., 2005; McGee et al., 2014; Chiessi et al., 2021), thereby reducing rainfall over northern Venezuela. However, modern marine sediment traps and continental shelf sediments show that regional rainfall amount is not always related to the amount of terrigenous material delivered to Cariaco (Peterson & Haug, 2006; Martinez et al., 2007), highlighting the importance of studying proxies that unambiguously reflect ITCZ-related convective activity, as has been proven for the millennial-scale events recorded in stalagmites from northeastern Brazil (Cruz et al., 2009; Utida et al., 2020).

Furthermore, there is a need for clarifying and filling major past hydroclimate data gaps that still exist in northern South America. Abrupt changes in precipitation linked to cooler North Atlantic SSTs during the iconic Holocene Bond events (Bond et al., 2001) have been identified in paleorecords as distant as Cuba in the northern Caribbean (Fensterer et al., 2013) and the region under the influence of the SAMS (Stríkis et al., 2011; Novello et al., 2012; Bustamante et al., 2016). However, such abrupt changes have not been reported in sites located under the direct ITCZ influence, which has prevented tracing the position of the ITCZ. For instance, low latitude manifestations of the 8.2 ka BP event indicate a dry period over the Caribbean (Haug et al., 2001; Lachniet et al., 2004; Fensterer et al., 2013), and intensification of the SAMS, as observed at mid-elevation in the Peruvian Andes (Bustamante et al., 2016) and in central/eastern Brazil (Cheng et al., 2009; Stríkis et al., 2011). In Venezuela, the Cariaco Ti record suggests highly variable but also slightly drier conditions between 8.3 and 7.8 ka BP (Haug et al., 2001). This is consistent with higher ratios of evaporation to precipitation (E/P) and/or higher salinity as inferred by the enriched ^{18}O in ostracods from Lake Valencia (1010^{0}N, 6745^{0}W, 400 masl) due to preferential evaporative loss of ^{16}O (Curtis et al., 1999). Unfortunately, comparisons with high-frequency changes in lake sediment proxies are difficult due to the lower resolution characterizing most of these records (Bradbury et al., 1981; Polissar et al., 2006, 2013) and their interpretations may be further complicated by past oscillations between closed and open hydrologic systems (Curtis et al., 1999).

Decreased (increased) precipitation associated with weaker (stronger) SAMS activity during the MCA (LIA) has been extensively delineated for southern tropical South America (Reuter et al., 2009; Bird et al., 2011; Kanner et al., 2013; Della Libera et al., 2022). Moreover, a weak SAMS during the MCA has been associated with a northerly position of the ITCZ in Cariaco (Haug et al., 2001; Vuille et al., 2012; Apaestegui et al., 2014; Novello et al., 2018). For the LIA, however, there is still little consensus in the literature on the paleo-hydrological conditions over Venezuela. Lake sediments from the Cordillera de Merida document glacial advances in the region prior to the onset of the LIA, supporting the prevalence of colder and wetter conditions (Polissar et al., 2006), while the opposite is recorded in Cariaco, where Ti concentration reached minimum values, suggesting drier conditions (Haug et al., 2001). Bird et al. (2018) argue for the possible influence of elevation-dependent terrestrial convection during the late-Holocene that reduced precipitation at frontal sites and increased it over the interior/Andean sites.

Here we present new speleothem records spanning the mid-and the late-Holocene from two different caves (Alfredo Jahn and Caripe, Fig. 1) located along northern Venezuela (less than 200 km from the Cariaco Basin). Based on modern $\delta^{18}O$ in precipitation data from the International Atomic Energy Agency/Global Network of Isotopes in Precipitation (IAEA/GNIP) (IAEA/WMO, 2021), and comparisons to other high-resolution time-series from the area, our Venezuelan speleothem isotopic records are interpreted to document the latitudinal ITCZ position in the past. Our new isotopic records provide relevant hydroclimatic information during the Holocene, allowing us to assess the local response to large scale multicentennial events, such as the 8.2 ka BP event, the MCA, the LIA and the Current Warm Period (CWP). A main goal of the present study is to investigate hitherto unreported secular- and multidecadal-scale climate variability within the region influenced by ITCZ migration, while interpreting this independent hydroclimatic reconstruction within a regional and global context.

2. Study site and modern climatology

Alfredo Jahn cave (10$28^0$45^{00}N, 66$16^0$24^{00}W, 210 masl) is located in the municipality of Brion, Miranda State, in the low-elevation foothills of the Serranía del Litoral (Central Coastal Cordillera, Fig. 1). It is hosted in calcitic and calcitic-dolomitic marbles of the Las Mercedes Formation of early Cretaceous age (Urbani, 1973; Forti et al., 1999). The thickness of the overburden above the cave varies between 10 and 30 m. Caripe cave is situated around 1100 masl, in the municipality of Caripe, Monagas State, to the south of the easternmost portion of the Cariaco Gulf, in the hills of the eastern Coastal Cordillera (Fig. 1). It is located at the top of a massive 170 m thick limestone sequence of the Guacharo Member in the El Cantil Formation of Aptian-Albian ages, and is 30e40 m below a broadleaf forest in the upper stratigraphic limit. The local vegetation of both Venezuelan caves is typical of a seasonal, semi-deciduous submontane ombrophilous broadleaf forest, inserted in desertic ecosystems with xerophytic shrubs (Gonzalez et al., 2008), making them highly sensitive sites to past narrowing of forest patches due to changes in precipitation.

The main atmospheric system that controls the annual cycle of rainfall over the region is the meridional migration of the ITCZ

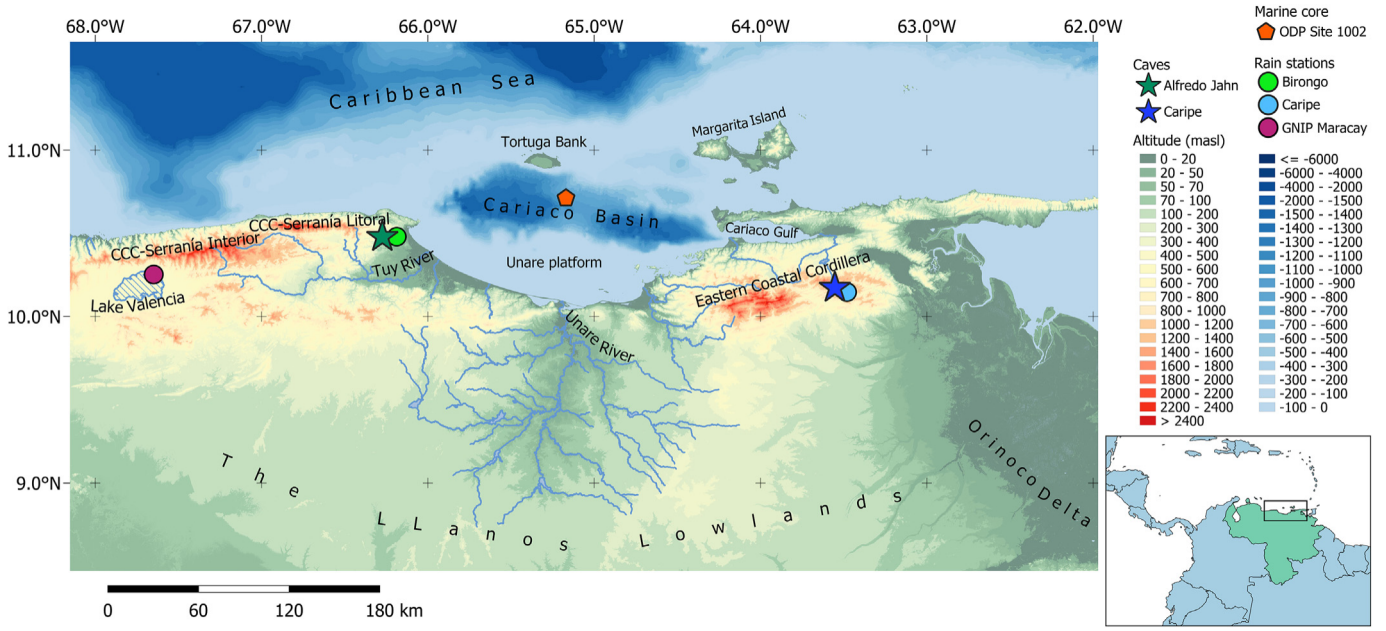

Fig. 1. Map of north central-eastern Venezuela showing the location of Alfredo Jahn (green star) and Caripe (blue star) caves, studied in the present work. The closest rainfall stations are also shown (blue and green circles, respectively), along with the Maracay GNIP station (pink dot) next to the Lake Valencia. Note the proximity of both caves to the Cariaco Basin. The location of marine sediment ODP Site 1002C (Haug et al., 2001) is shown (orange hexagon) to represent one of the many cores retrieved from the central saddle of the Basin. CCC: Central Coastal Cordillera. Digital elevation model (DEM) is from NASA Shuttle Radar Topography Mission. The bathymetry is from GEBCO Digital Atlas published by the British Oceanographic Data Centre. Map created using the free and open source QGIS.

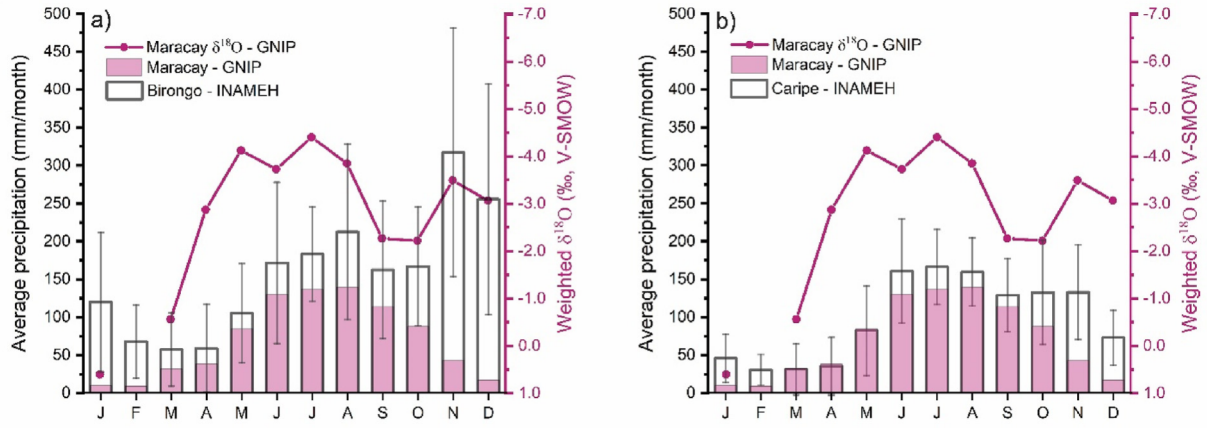

Fig. 2. Monthly mean precipitation for GNIP and INAMEH meteorological stations located close to cave sites a) Alfredo Jahn cave: Maracay and Birongo. b) Caripe cave: Maracay and Caripe. Weighted $\delta^{18}O$ oxygen isotope ratios for Maracay (1961e1975) were calculated from GNIP IAEA/WMO database (IAEA/WMO, 2021). Birongo (1951e1954, 1960e1999) and Caripe (1960e2007) data are from INAMEH (Instituto Nacional de Meteorología e Hidrología, Venezuela). Note that the scale for right-side y-axis ($\delta^{18}O$) is inverted in the two panels. There is no $\delta^{18}O$ data for February.

(Figs. 2e3) (Pulwarty et al., 1992; Poveda et al., 2006), resulting in distinct dry and wet seasons. The dry season occurs from January to March, when the ITCZ is located in its southernmost latitudinal range over northeastern Brazil. Most of the rain tends to fall during June-July-August, following the local North American monsoon (Jin et al., 2020; Liu et al., 2022), when the ITCZ is directly overhead (Lea et al., 2003; Peterson & Haug, 2006). The wet season may extend until NovembereDecember in some windward regions due to their exposure to moisture-laden trade winds, as is the case at Birongo and Caripe, the closest meteorological stations to the Alfredo Jahn and Caripe caves (Fig. S1). Mean annual rainfall is 1862 ± 414 mm and 1146 ± 202 mm at those two sites, respectively, and 85% and 88% of it falls during the long-wet season from May to December.

Despite the more seasonal precipitation pattern (Table S1, Fig. S2), Maracay GNIP $\delta^{18}O$ rain values also differ between a short dry and extended wet season. Heavy $\delta^{18}O$ values between 0.5 and 0.5‰ are observed during January and March (Fig. 2) which can in part be explained by partial evaporation of light rains in tropical North Atlantic source areas (Rozanski et al., 1993; Fröhlich et al., 2002). More negative rain water isotopic values occur from April to December, varying between 2.5 and 4.5‰ (Fig. 2). The data indicate a seasonal variation of the isotopes in precipitation, while intraseasonal patterns, especially during the wet season, may require further investigation.

3. Samples

Venezuelan speleothems VEAJ from Alfredo Jahn cave and VECA from Caripe cave were used in this study. VEAJ is a 340 mm-long stalagmite that grew in three major parts (Fig. 4). The lower section

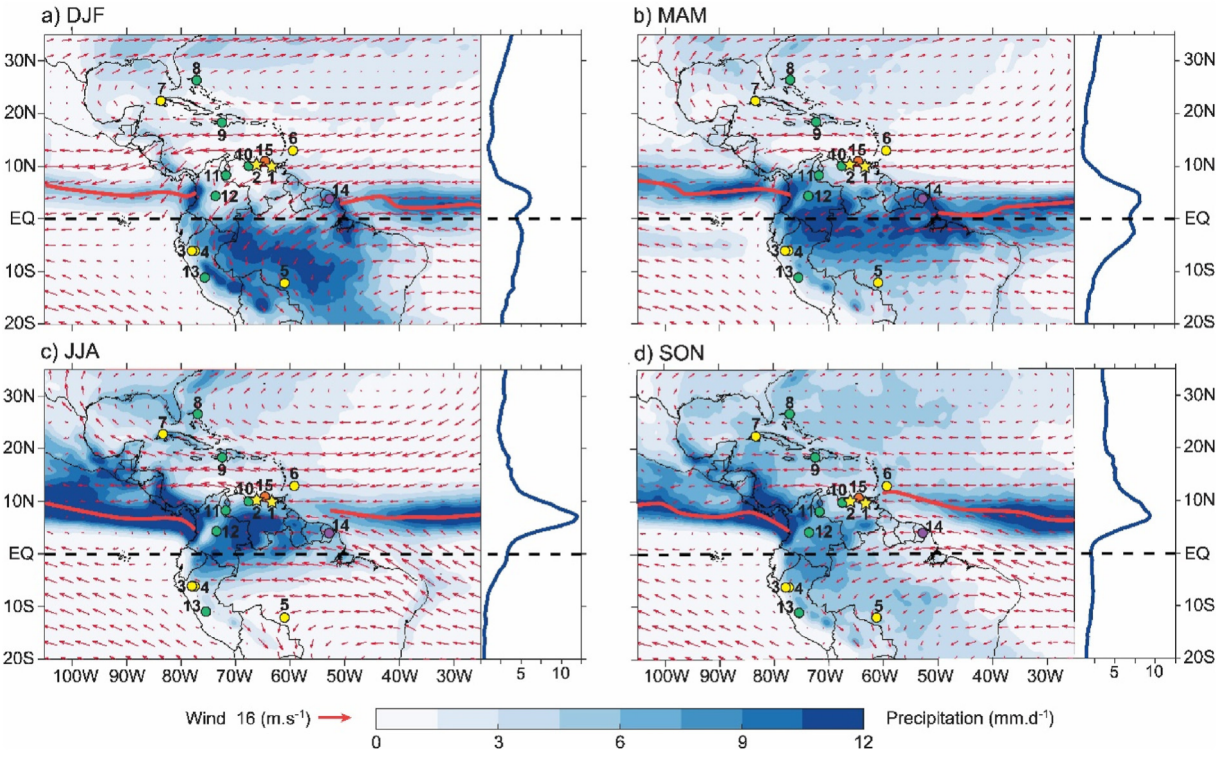

Fig. 3. Seasonal mean precipitation in mm d^{1} from 2001 to 2020 based on Global Precipitation Measurement (GPM) data (Huffman et al., 2019) (blue shading) and seasonal mean low-level wind circulation in $m.s^{1}$ at 850 hPa from 2001 to 2020 from ERA5 (red vectors). Yellow stars: this study (1e2). Circles represent records discussed in the text (yellow: caves 3e7; green: lakes 8e13; purple: swamp 14; orange: marine sediment records 15). The red line marks the approximate position of the ITCZ, based on the meridional maximum precipitation values. The blue line in the panels to the right marks the zonally-averaged precipitation (mm/day) as a function of latitude for each season evaluated. Black dashed line indicates the equator. Numbering corresponds to: 1) Alfredo Jahn (VEAJ, north-central Venezuela); 2) Caripe (VECA, northeastern Venezuela); 3) Shatuca (SHA-2 & SHA-3, Peru) (Bustamante et al., 2016); 4) Palestina (PAL, northern Peru) (Apaestegui et al., 2014); 5) Cuíca (PIM4 & PIM5, western Brazil) (Della Libera et al., 2022); 6) Harrison (HC-1, Barbados) (Mangini et al., 2007); 7) Dos Anas (CP, northwestern Cuba) (Fensterer et al., 2013); 8) Great Cistern sinkhole (Bahamas) (Sullivan et al., 2021); 9) Lake Miragoane (Haiti) (Hodell et al., 1991); 10) Lake Valencia (north-central Venezuela) (Curtis et al., 1999); 11) Laguna Blanca (northwestern Venezuela) (Polissar et al., 2013); 12) Laguna de Ubaque (central Colombia) (Bird et al., 2018); 13) Pumacocha (central Peru) (Bird et al., 2011); 14) Les Nouragues swamp (French Guiana) (Ledru, 2001); 15) Cariaco Basin (Venezuela) (Peterson et al., 1991; Hughen et al., 1996; Black et al., 1999; Haug et al., 2001; Gibson and Peterson, 2014).

(VEAJ-base) grew first and has a number of axes that are slightly shifted to the sides, likely as a result of drip realignments due to overburden changes, seismic activity, or perhaps due to the opening of new adjacent dripping ducts as the central one got sealed. Two adjacent stalagmites grew on the top of the base: the top left (VEAJ-top left, green outline) and top right (VEAJ-top right, pink outline), are also characterized by significant changes in axial position (Fig. 4).

Sample VECA is a 314 mm long stalagmite. The first 191 mm from the base underwent dissolution and reprecipitation of carbonate in the central portion, leading to a vitreous luster that contrasts with the pristine white-colored layers to the sides (Fig. 5). Most of the dating analyses in this lower white section did not show age inversions, further supporting the visual characterization of the unaltered layers (Fig. 5).

4. Methods

4.1. UeTh dating and depth-age modeling

The majority of UeTh dating was performed at the Institute of Global Environmental Change at Xi'an Jiaotong University in China. A few additional samples were analyzed at the University of Minnesota (USA) (Tables S2e3). In both cases multicollector inductively-coupled plasma mass spectrometers (MC-ICP-MS-Thermo-Finnigan NEPTUNE) were operated following the procedures of Cheng et al. (2013). A handheld drill was used to take approximately 0.100 g of the least porous and colored, most traceable layers along or at the side of the growth axis (gray line) (Figs. S3e4). Age model chronologies for speleothem samples were constructed using the StalAge algorithm developed by Scholz and Hoffmann (2011). Several age reversals along stalagmite VEAJ were noted (Fig. 4). Some of them, using Bayesian statistics, were flagged as outliers and consequently removed from the age models. For other age inversions, an iterative procedure was applied to increase the range of uncertainty in order to fulfill the monotonicity criterion (Scholz and Hoffmann, 2011). Also, for the VECA sample a few outliers were removed, while for other age reversals the error was enlarged (Fig. 5).

4.2. Stable isotope analyses and VEAJ-top composite

Approximately 200 mg of $CaCO_3$-powder subsamples for $\delta^{18}O$ and $\delta^{13}C$ stable isotopic analyses were collected using a manually controlled Sherline 5400 milling at a resolution of 0.4 mm for VEAJ (Figs. 4c) and 0.5 mm for VECA samples (Fig. 5b). Isotope analyses were determined on an Isotope Ratio Mass Spectrometer (IRMS) coupled to a Gas Bench II at the Geoscience Institute at the University of São Paulo, Brazil (LES-CPGeo). δ-notation in per mil units (‰) was used to express the sample isotopic ratios deviation from the Vienna Pee Dee Belemnite (VPDB) standard. The $\delta^{18}O$ and $\delta^{13}C$ isotopic profiles of VEAJ-base, VEAJ-top left and VEAJ-top right are based on 530, 310 and 250 samples, respectively. VECA isotopic profiles consist of 670 samples. Since VEAJ-top left overlaps with

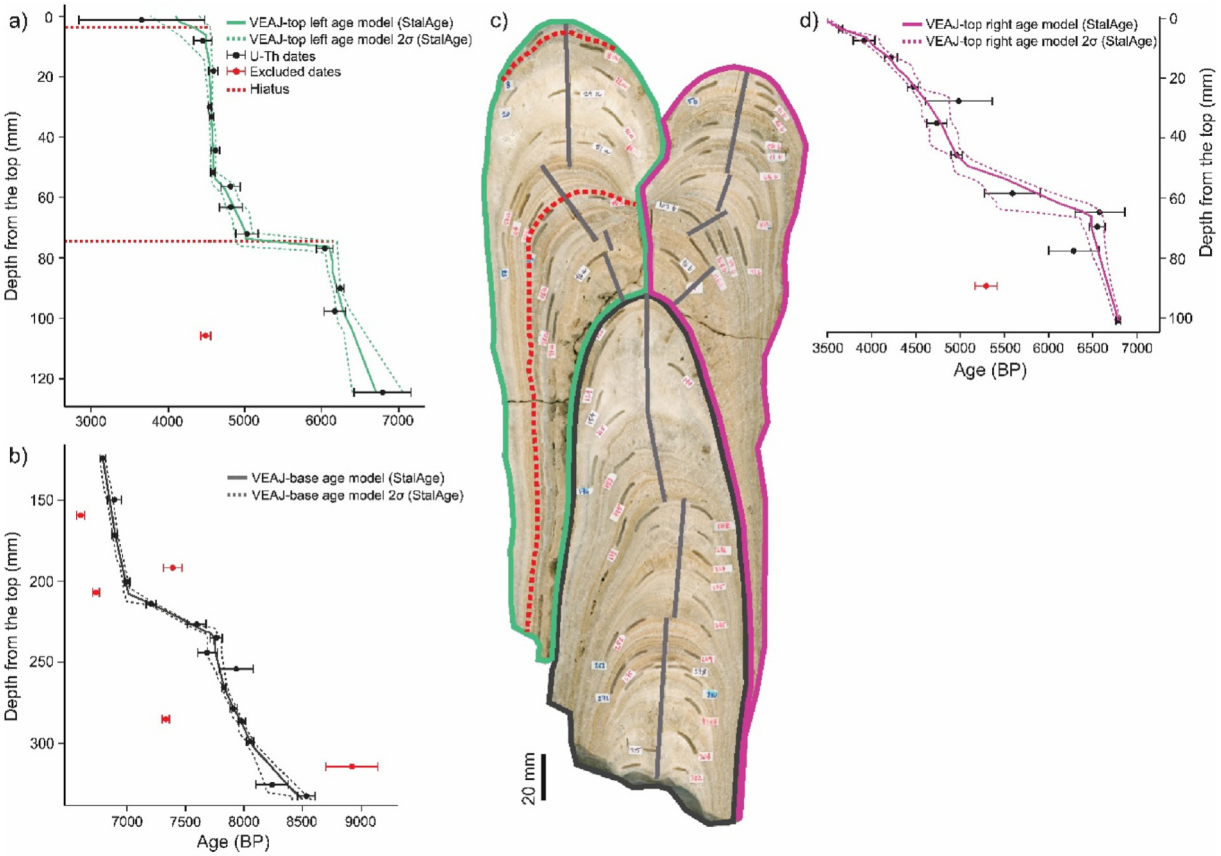

Fig. 4. Age-depth model for Alfredo Jahn cave speleothem VEAJ (north-central Venezuela) with three main growth axes: a) VEAJ-top left (green line with the red dashed lines indicating hiatuses). b) VEAJ-base (dark gray line) and d) VEAJ-top right (pink). Age-depth models were obtained with the StalAge algorithm (Scholz and Hoffmann, 2011). Associated 95% confidence intervals for each age model are shown as dashed lines. Circles and error bars represent UeTh dates. Red circles are outliers discarded in the age models. c) VEAJ sample with the color outlines as described above, enclosing the major three growth axes. Milling channels for stable isotopes are shown in gray. Hiatuses identified in the age-depth model are also shown as red dashed lines.

some sections of the -top right record (Figs. S5e6), we merged them by using a statistical procedure (see supplementary text S2). The record composed of the merged segments and the remaining -top right record is henceforth referred as VEAJ-top composite.

5. Results

Sample VEAJ (VEAJ-base & top-composite), covers without interruption 5000 years of the Holocene (3.5e8.5 ka) (Fig. 6). Notably, growth rates were higher in the base stalagmite (up to 0.5 mm/yr) than in the top composite (up to 0.08 mm/yr), providing mean temporal stable isotope sampling resolutions of 3 and 23 years, respectively. Sample VECA from the higher elevation Caripe cave covers the last 2250 years, which complements the record from Venezuela, except for three hiatuses of 280, 135 and 270 years, between 1720 and 1440 BP (230e510 CE), 875-740 BP (1075e1210 CE) and 430-160 BP (1520e1790 CE), respectively (Fig. 7).

VEAJ $\delta^{18}O$ values range between 2.5 and 4.6‰ (average ¼ 3.6‰) and $\delta^{13}C$ between 6.3 and 11.8‰ (average ¼ 9.8‰). $\delta^{18}O$ and $\delta^{13}C$ are positively correlated (r ¼ 0.6, p-value<0.1). The $\delta^{18}O$ time-series show a distinctive 506-yr oscillatory pattern (95% statistical confidence) with superposed multidecadal variations (Fig. S7) and a slight trend toward lower values between 8.4 and 6.5 ka BP (Fig. 6). In VEAJ, both $\delta^{18}O$ and $\delta^{13}C$ (Fig. 6) are punctuated by anomalous higher values around 8.4e8.1, 7.6, 7.3e7.2, 6.8, 6.6, 6.4e6.2 ka BP, and anomalous lower values at 8.5, 8.0, 7.8, 7.6e7.4, 7.0, 6.7, 6.5, 6.0 ka BP. From 6.0 to 5.0 ka BP, a trend toward higher $\delta^{18}O$ values was marked by a maximum in both $\delta^{18}O$ and $\delta^{13}C$ records at 5.2 ka BP. Afterwards values became progressively depleted in heavy isotopes from 4.9 to 4.2 ka BP, when they again started to become gradually more enriched until 3.6 ka BP.

The Caripe cave sample (VECA) shows a lower mean value and a larger $\delta^{18}O$ isotopic range (between 2.5 and 5.3‰, average ¼ 3.9‰) than VEAJ (Fig. 7). Growth rates were higher in the oldest portion of the stalagmite, which resulted in an average resolution of 1.5 years. The following two periods and the youngest segment feature an average resolution of 4 and 16 years, respectively. A remarkable 41-yr periodicity within 95% statistical confidence was present along the oldest segment from 2250 to 1720 BP (300 to 230 CE) (Fig. S8). Oscillations in this segment mostly occur close to the mean, however, high amplitude variability was observed between 2030 and 1830 BP (80 BCE and 120 CE). After the first hiatus, a period of lower $\delta^{18}O$ values was observed between 1450 BP (500 CE) and 1250 BP (700 CE) (4.7‰). This was followed by a $\delta^{18}O$ increase of ~1.5‰, which lasted until the beginning of the MCA at 1050 BP (900 CE) (Fig. 7a). The MCA (1050e850 BP/900 to 1100 CE, red shading) was characterized by higher $\delta^{18}O$ values (3.8‰), than the previous period from 1450 to 1250 BP, and was punctuated by two abrupt heavy isotope enrichments centered at 1010 BP (940 CE) (3.3‰) and 940 BP (1010 CE) (3.0‰). Spectral analysis of this segment indicates periodicities centered on 70, 12 and 9 years, within 95% statistical confidence (Fig. S9). The following youngest segments of the record are too short for

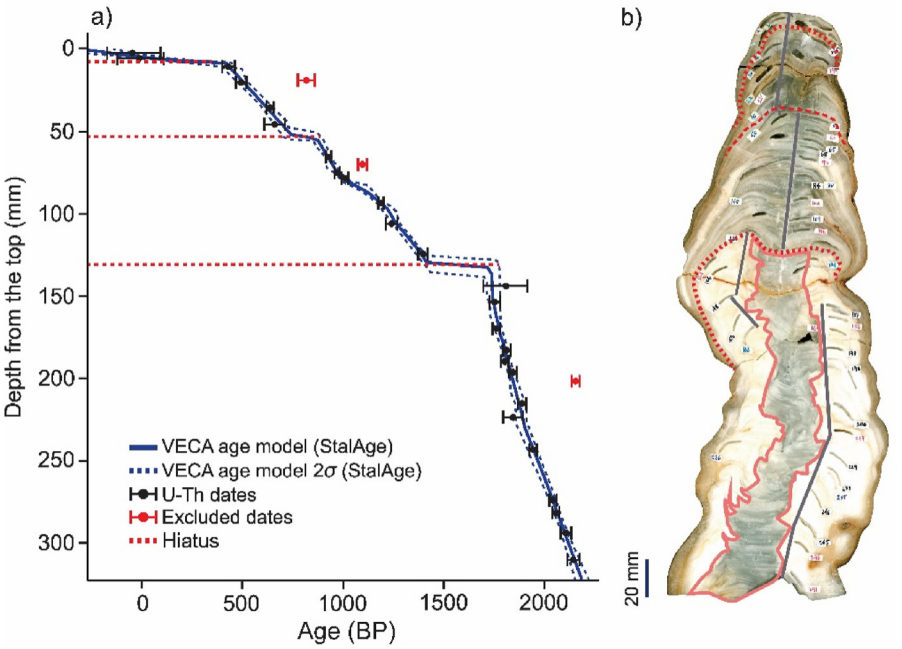

Fig. 5. Age-depth model for Caripe cave speleothem VECA (northeastern Venezuela) obtained with the StalAge algorithm (Scholz and Hoffmann, 2011). a) Age-depth model for VECA (navy blue line) and its associated 95% confidence interval (navy blue dashed lines). Circles and error bars represent UeTh dates. Red circles are outliers that were discarded in the age model. b) Caripe cave speleothem with the milling channels for stable isotopes in gray. Pink color outline encloses the vitreous portion that suffered dissolution and reprecipitation. Hiatuses identified in the age-depth model are shown as red dashed lines in both panels.

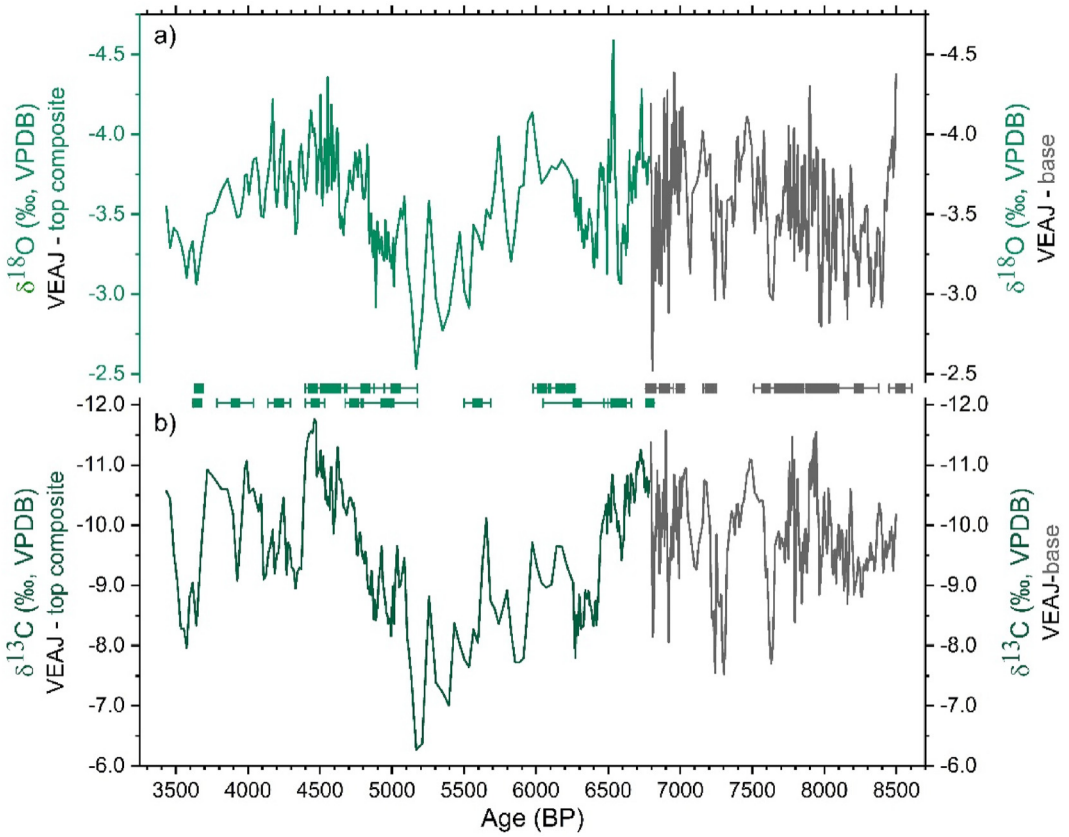

Fig. 6. a) $\delta^{18}O$ and b) $\delta^{13}C$ isotopic profiles and UeTh dates along the VEAJ three major growth axes: VEAJ-base, VEAJ-top left, and VEAJ-top right. Since top left overlaps the top right record, we merge these sections by using a statistical procedure. The merged sections together with the remaining VEAJ-top right record are referred here after as VEAJ-top composite (curves in green). Note that scale for all y-axes is inverted.

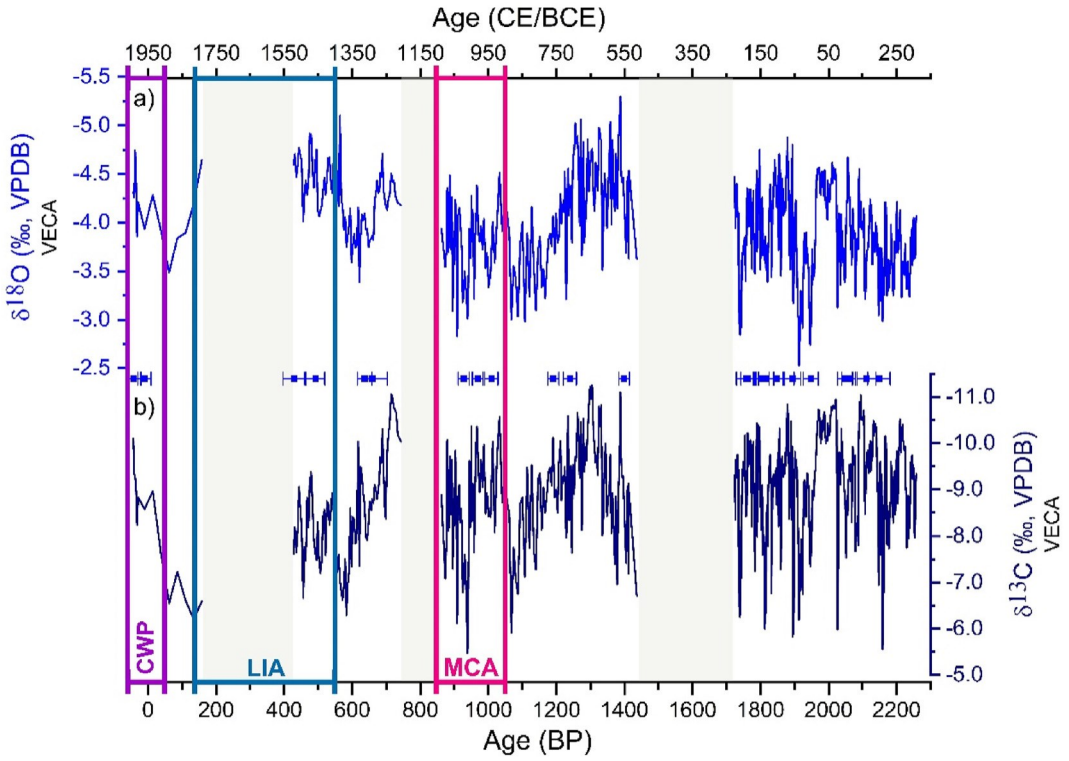

Fig. 7. a) $\delta^{18}O$ (navy blue) and b) $\delta^{13}C$ (dark blue) isotopic profiles of Caripe Cave VECA sample. UeTh dates with their corresponding error bars are also shown. The three hiatuses are indicated in gray shading. Red, blue and purple boxes represent the MCA (1050e850 BP/900e1100 CE), the LIA (550e130 BP/1400e1820 CE) and the CWP (50 BP- today/1900 CE-today) periods as defined in Bird et al. (2011), respectively. Note that the scale for both y-axes is inverted.

conducting spectral analysis. However, they show an increase of ~1.0‰, just before the onset of the LIA (550e130 BP/1400e1820 CE, blue shading), followed by a trend toward lower values from 575 BP (1375 CE) until 435 BP (1515 CE) (4.5‰) (Fig. 7). During the period corresponding to the CWP, a trend toward lower values was observed from 60 BP (1890 CE) until the end of the record at 1990 CE. $\delta^{13}C$ is positively correlated with $\delta^{18}O$ through the entire record ($r = 0.56$, p-value<0.05).

6. Basis for interpretation of $\delta^{18}O$ values

The stable isotope composition of local precipitation is controlled by regional-scale processes such as the total precipitable water, amount effect, rainout upstream (in marine and continental settings) and evapotranspiration (Dansgaard, 1964; Rozanski et al., 1982, 1993; Vuille et al., 2003). Back-trajectory analyses (Figs. S10e11) show that moisture transport associated with precipitation at our study sites is mainly sourced from the tropical Atlantic Ocean. Hence, due to the prevalent influence of north-eastern trade winds on regional precipitation, and the proximity of our caves to the coastal region, there is no significant moisture path located over the continent. Therefore, we argue that isotopic modifications by upstream convection and recycled moisture by evapotranspiration are of minor importance. Indeed, the rainout effect becomes more dominant further inland (Vuille et al., 2003; Della Libera et al., 2022). Rather, north central-eastern Venezuelan precipitation $\delta^{18}O$ values reflect the seasonal variability of precipitation amount following the prevailing circulation patterns in the atmosphere. From January to March, a dry, cold winter atmosphere and strengthened trade winds result in high $\delta^{18}O$ rainwater values, due to the reduction of the total precipitable water and the partial evaporation of light rains (Rozanski et al., 1993; Fröhlich et al., 2002). As the months progress to summer, the ITCZ displaces northward following the Northern Hemisphere warming, and the total precipitable water increases. The lowest $\delta^{18}O$ values and higher precipitation amounts at our cave sites are observed during June-July-August, when moisture convergence associated with the ITCZ maximizes over the continent at 10N. The dominant rainout process from deep convective clouds embedded in the ITCZ results in increasingly ^{18}O-depleted precipitation (Dansgaard, 1964; Vuille et al., 2003).

Correlations between precipitation totals and weighted-$\delta^{18}O$ values are, as expected, negative at annual scales for Birongo (0.54, p-value ¼ 0.09, n ¼ 11), Caripe (0.22, p-value ¼ 0.49, n ¼ 12) and Maracay (0.42, p-value ¼ 0.18, n ¼ 12). The correlation is significant at p-value<0.1 at Birongo, but not at Caripe and Maracay. The amount effect is not as evident as at some other tropical locations but this is likely due to the low number of data points. Nevertheless, on annual to longer scales, the amount effect is likely the main control of isotope values in precipitation in northern Venezuela as has been widely suggested for tropical regions and especially for those located at maritime or nearby-coastal sites (Dansgaard, 1964; Rozanski et al., 1993; Vuille et al., 2003; Fairchild et al., 2006).

ENSO may at times have exerted a significant influence on the hydroclimatic variability at our study sites, especially over the Late Holocene (Clement et al., 1999; Moy et al., 2002; Conroy et al., 2009), as suggested by the higher variability in the VECA record relative to the mid-Holocene VEAJ record. However, most of the variability at our sites is driven by the Atlantic and much of the ENSO signal in this region is also communicated via teleconnections through the tropical North Atlantic.

7. Discussion

7.1. Relationship with the Cariaco Basin records

The Ti concentration (Haug et al., 2001) and gray-scale (Hughen et al., 1996) data from Cariaco are interpreted as proxies of the ITCZ position through continental runoff and the relative deposition of marine vs. terrestrial sediments, respectively (Fig. 8a,c). Our records may not be suitable for tracking the long-term trend associated with insolation as seen in the Ti record, because they are based on speleothem samples from two different caves. On the other hand, they show high-frequency variability that is not apparent in the Cariaco records (Fig. 8b). This comparison suggests that Ti concentration and gray-scale might be also influenced by other factors (e.g. ocean circulation and sea level) (Peterson & Haug, 2006; Martinez et al., 2007), masking the high-frequency signal from precipitation variability over the region. There are some exceptions to this behavior, such as the subtle drying seen from 8.3 to 8.0 ka BP, coinciding with the 8.2 ka BP event. Nonetheless, the high-amplitude climate variability observed in our $\delta^{18}O$ VEAJ record from 8.0 to 4.0 ka BP has no counterpart in the Ti and gray-scale records (Fig. 8). However, other Cariaco records that have been less explored in the literature for the Holocene period (Fig. S12), better mirror the variability detected in our new $\delta^{18}O$ speleothem time series and might require further investigation.

7.2. Tracking the mid-Holocene ITCZ position

A detailed comparison between high-resolution records from the tropical Americas, including the Great Cistern sinkhole (Bahamas, Sullivan et al., 2021), CP (northern Cuba, Fensterer et al., 2013), VEAJ (north-central Venezuela, this study), HC-1 (Barbados, Mangini et al., 2007) and SHA-2 & SHA-3 (northwestern Peru, Bustamante et al., 2016) provides information on the mean latitudinal position of the ITCZ during the mid-Holocene (Fig. 9ceh). Indeed, around 8.2 ka BP, a southern position of the ITCZ relative to northern Venezuela (Fig. 9g) coincides with a relatively wet period in Peru (Fig. 9h). However, none of those changes were as abrupt as the dry period observed in Cuba (Fig. 9e). From 8.0 to 6.5 ka BP, Venezuela and Cuba became progressively wetter (Fig. 9e,g); a trend that has been widely observed in Caribbean records that span the early Holocene and has been associated with increased Northern Hemisphere (NH) insolation (Hodell et al., 1991; Curtis et al., 1999; Fensterer et al., 2013). During this period the ITCZ might have been displaced farther north during boreal summer and farther south during the boreal winter due to high interhemispheric surface temperature gradients (Hastenrath, 1984; Hodell et al., 1991; Coe and Bonan, 1997; Campos et al., 2022). The mean position of the North Atlantic Subtropical High (NASH) might also have been displaced northward, driving sustained divergence over the Bahamas (Sullivan et al., 2021) (Fig. 9c).

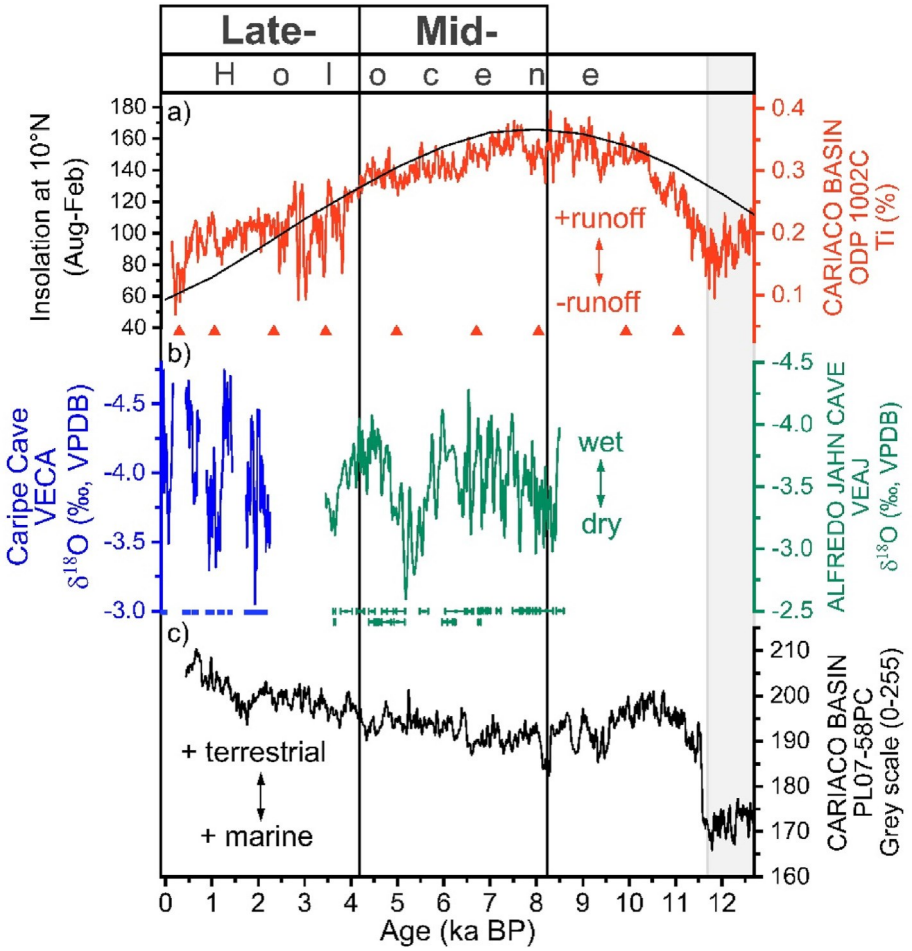

Fig. 8. Cariaco Basin a) Ti concentration (%, orange) (Haug et al., 2001) and c) gray-scale (0e255, black) (Hughen et al., 1996), compared to b) our speleothem $\delta^{18}O$ records from Alfredo Jahn (‰, green) and Caripe caves (‰, blue). The data were filtered using a 20-yr running mean. Note that the scale for both $\delta^{18}O$ y-axes is inverted. The black line in a) represents the difference in insolation at 10N between the months of August and February (Berger and Loutre, 1991), which is a measure of the intensity of the annual cycle (Hastenrath, 1984; Hodell et al., 1991). The gray shading represents the Younger Dryas period.

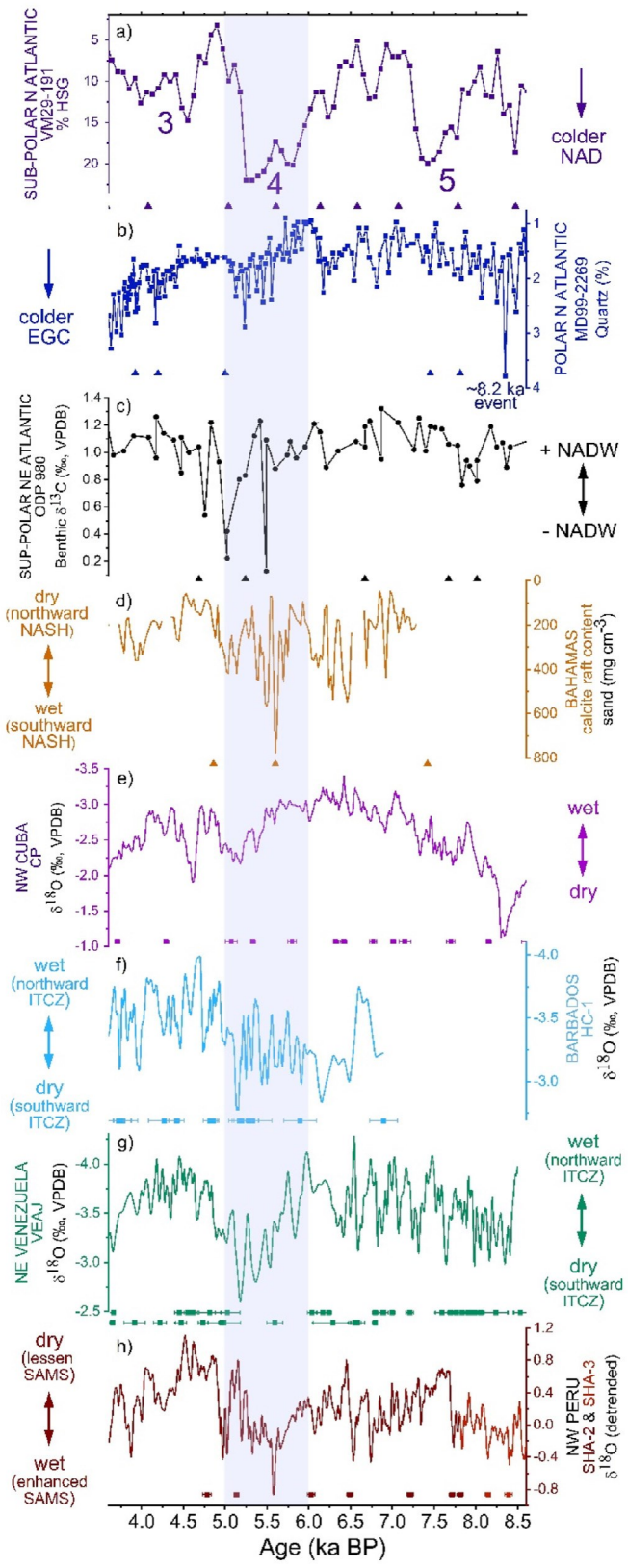

Fig. 9. Comparison of Holocene records spanning the period between 8.6 and 3.6 ka BP: a) ice-rafted debris (hematite-stained grains HSG) to the warm North Atlantic Drift (NAD) (dark purple, Bond et al., 2001); b) ice-rafted debris (%quartz) to the cold East Greenland Current (EGC) (dark blue, Moros et al., 2006); c) NADW circulation (epifaunal benthic foraminifera Cibicidoides wuellerstorfi $\delta^{13}C$ carbon isotope composition) (black, Oppo et al., 2003); d) NASH position (calcite raft content sand in mg cm^3) (orange, Sullivan et al., 2021); and high-resolution speleothem $\delta^{18}O$ (‰ VPDB) records: e) CP, northern Cuba (purple, Fensterer et al., 2013); f) HC-1, Barbados (light blue, Mangini et al., 2007); g) VEAJ, north-central Venezuela (jade green, this study) and h) SHA-2 and SHA-3, northwestern Peru (wine and red, Bustamante et al., 2016). Corresponding ages with error bars are shown. A 25-yr running average has been applied to the speleothem records from e) to h). Note that the scale for $\delta^{18}O$ y-axes is inverted, except for the detrended Peruvian time series in order to highlight the inferred relationship between the southward (northward) shift of the ITCZ and moisture funneling (deficit) toward the SAMS domain.

Between 6.0 and 5.0 ka BP, drying trends are observed in Cuba, Venezuela and Barbados (Fig. 9e,g-h). This can be attributed to a southward displacement of the NASH and the ITCZ. During this period, peak dry conditions coincide within age uncertainties in the records and occur around 5.2 ka BP (Fig. 9eeg). At about the same time, convection over the SAMS domain increased as evidenced by more negative $\delta^{18}O$ values between 5.5 and 5.0 ka BP in the Peruvian record (Bustamante et al., 2016), except for the $\delta^{18}O$ peak centered at 5.2 ka BP (Fig. 9h). This event suggests that other factors aside from the southward displacement of the ITCZ affected climate at the time and led to the abrupt precipitation anomalies recorded in the mid-elevation Peruvian Andes. Still, the similar magnitude and duration of this long-term change and increased drift ice (Bond et al., 2001; Moros et al., 2006), suggest a North Atlantic forcing of tropical American hydroclimate during this period (Fig. 9a and b) (see an in-depth discussion in the next section). After 4.9 ka BP, a sustained wet period occurred until 4.2 ka BP in both Venezuela and Barbados, revealing a northward ITCZ position (Fig. 9f and g), coincident with a reduction in convective activity over the SAMS region (Fig. 9h). From 4.1 to 3.6 ka BP, a trend toward drier conditions again points to a southward displacement of the ITCZ and an enhancement of the SAMS (Fig. 9feh).

7.3. North Atlantic influence on ITCZ position during the mid-Holocene

Inferred dry (wet) conditions in our VEAJ north-central Venezuela record during the mid-Holocene appear to be synchronous with an increased (decreased) drift ice input to the cold East Greenland Current (EGC) (Fig. 9b,g). An isotopic response to the sea ice advected to the North Atlantic Drift (NAD) (i.e. where the classical Bond events were described in marine core VM29-191) is less apparent, except for the strongest of the cold events (Bond 4) between 6.5 and 5.0 ka BP (Bond et al., 2001) (Fig. 9a,g). Indeed, during this period, the increase in sea ice advection to both the cold EGC (Moros et al., 2006) and the warm NAD (Bond et al., 2001) coincides with major drying in Venezuela, also apparent in other eastern Caribbean records (e.g. Great Cistern sinkhole, CP and HC-1). It has been suggested that a severe reduction of the NADW production occurred during this interval, as inferred from the low $\delta^{13}C$ values of benthic foraminifera at the Feni Drift in the subpolar northeastern Atlantic (Oppo et al., 2003) (Fig. 9c). This linkage between fresh-water input via massive icebergs discharge, reduction of the NADW production, weakening of the AMOC and southward migration of the ITCZ has been widely described for peak stadials and Heinrich events (Lea et al., 2003; Deplazes et al., 2013; Bohm et al., 2015; Mulitza et al., 2017), and validated by a suite of ocean-atmosphere general circulation modeling studies (Vellinga and Wood, 2002; Marcott et al., 2011). But a paleoclimate archive that recorded the response of the ITCZ to changes in the North Atlantic circulation during the relatively stable Holocene period has been missing.

The North Atlantic climate anomalies are rapidly transmitted to the tropics via atmospheric circulation changes (Chiang and Bitz, 2005). Hence, the synchronicity between the rise in polar and

sub-polar ice-rafted debris and the start of northeastern Venezuela drying around 6.0 ka BP might be a result of the wind-evaporation-SSTs feedback (WES) (Chiang and Bitz, 2005). A southward displacement of the NASH (Fig. 9d) might have triggered stronger trade winds and displaced the ITCZ to the south, in a way similar to today's boreal winter conditions (O'Brien et al., 1995; Oppo et al., 2003; Jackson et al., 2005). Between 5.5 and 5.0 ka BP, the decrease in the oceanic heat transport to the NH, linked to the reduction of NADW production, might have resulted in an even stronger southward displacement of the ITCZ, as inferred by the highest values of our Venezuelan record (Fig. 9f). Higher-frequency variability between 8.5 and 6.5 observed in the VEAJ record might also indicate subtle changes in drift ice input to the EGC and accompanying reductions in NADW (Fig. 9bec,g).

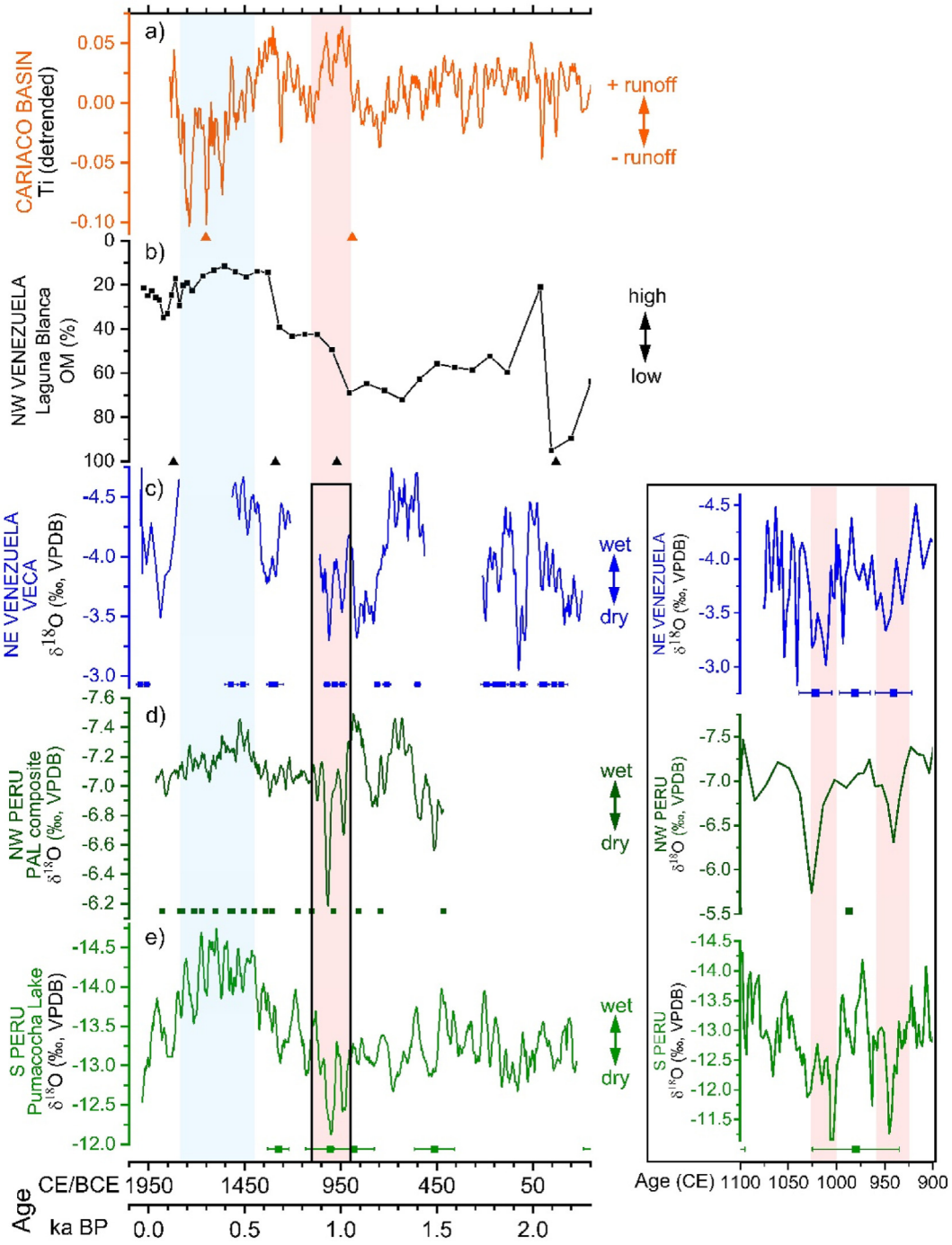

Fig. 10. Comparison of the climate during the last 2300 years based on a) detrended Ti record from Cariaco Basin (orange, Haug et al., 2001), and speleothem and lake records from b) northwestern Venezuelan Merida Andes Laguna Blanca (OM%) showing lake level variations (black, Polissar et al., 2013) c) northeastern Venezuela VECA ($\delta^{18}O$, ‰ VPDB) (blue, this study), d) northwestern Peru PAL composite ($\delta^{18}O$, ‰ VPDB) (dark green, Apaestegui et al., 2014), and e) central Peru Pumacocha Lake ($\delta^{18}O$, ‰ VPDB) (green, Bird et al., 2011). Red, blue and purple shading in the left panel represent the MCA (1050e850 BP/900e1100 CE), the LIA (550e130 BP/1400e1820 CE) and the CWP (1900-today) periods as defined in Bird et al. (2011), respectively. A 20 to 25-yr running average has been applied to the records (cee). Inset f) is an expanded view into the MCA with the red shading showing periods of anomalous increase in $\delta^{18}O$ values. Note that the scale for all the $\delta^{18}O$-speleothem records is inverted. Dates with error bars are displayed. Ages for the top 103.5 cm in the Pumacocha record are based on layer counting.

7.4. The MCA, LIA and CWP in northeastern Venezuela

Our northeastern Venezuela VECA record of the last 2300 years from Caripe cave differs considerably from the Cariaco Ti record (Haug et al., 2001) (Fig. 10a,c) And coincides with hydroclimate conditions inferred by some Venezuelan lake proxy records (Fig. 10b) (see discussion of northern South America lake proxy records in supplementary text S6, Figs. S13e16). Prior to the MCA, precipitation in northeastern Venezuela appears to have been high, similar to most of the SAMS domain (Della Libera et al., 2022) (Fig. 10cee). During most the last 1000 years, our VECA speleothem record closely resembles the western tropical South American records (Bird et al., 2011; Apaestegui et al., 2014; Della Libera et al., 2022) (Fig. 10c and d), with a relatively dry (wet) mean state during the MCA (first part of the LIA) in northeastern Venezuela (Fig. 10b). We suggest that following the anomalously warm temperatures observed in the NH during the MCA (1050-850 BP/ 900e1100 CE) (Moberg et al., 2005; Mann et al., 2009), the ITCZ was located to the north of northern Venezuela, which led to the observed relatively high $\delta^{18}O$ values and the in-phase relationship with the tropical Southern Hemisphere (SH) South American records. Moreover, when looking at decadal scales, our VECA record also shows the distinctive "double-peak" structure of higher $\delta^{18}O$-values (around 940 and 1010 CE), first documented in Bird et al. (2011) and extensively described in Apaestegui et al. (2014) (Fig. 10e). As in the record from Palestina Cave, we also found a significant periodicity centered around 70 yrs within 95% statistical confidence during the MCA (Fig. S9), supporting the notion of a positive AMO phase as the main forcing mechanism of those dry events (Mann et al., 2009; Novello et al., 2012; Apaestegui et al., 2014). This explanation is also consistent with an even farther northward migration of the ITCZ, away from northern Venezuela, resulting in even drier conditions at our study site during positive AMO phases.

Conversely, relatively lower $\delta^{18}O$ values are observed in our VECA record during the first part of the LIA (550-450 BP/ 1400e1500 CE), similar to what is observed over the core monsoon region (Fig. 10), pointing to a mean ITCZ position near the equator, likely over the Guianas. This ITCZ displacement led to enhanced moisture influx over the eastern portion of Venezuela, while also enhancing moisture convergence over the SAMS region. Cold conditions, likely due to stronger winds (Black et al., 1999), might have prevailed during this period, leading to open vegetation and heavier $\delta^{13}C$ values in Caripe, as also indicated by the persistence of the pioneer species Cecropia in pollen records from French Guiana (Ledru, 2001), glacial advances in the Cordillera de Merida (Polissar et al., 2006) and reduced charcoal abundance in Lake Valencia (Curtis et al., 1999). During the main LIA period, however, the ITCZ position might have migrated further south, greatly enhancing the monsoon over the western Amazon Basin and central Peru (Bird et al., 2011; Della Libera et al., 2022), while resulting in a depositional hiatus in our VECA speleothem (Fig. 5), consistent with drier conditions in the circum-Caribbean (Hodell et al., 2005; Lane et al., 2011; Winter et al., 2011; Fensterer et al., 2012). Finally, the most recent warming (CWP) since the start of the industrial revolution is expressed in northeastern Venezuela as a rapid change toward wetter conditions since 1890 CE, contrasting with the trend toward drier conditions in the SAMS domain (Bird et al., 2011; Vuille et al., 2012). This is consistent with the global monsoons hemispheric asymmetry, driven by the enhanced warming in the NH relative to the SH associated with anthropogenic climate change.

8. Conclusions

Based on the available monitoring data (IAEA/WMO, 2021), back trajectory analyses, and the coherence with other paleoclimatic records from tropical and subtropical America (Mangini et al., 2007; Bird et al., 2011; Fensterer et al., 2013; Apaestegui et al., 2014; Bustamante et al., 2016; Sullivan et al., 2021) we interpret $\delta^{18}O$ isotopic variability in Venezuelan speleothems covering most of the Holocene as reflecting the proximity of the ITCZ convective activity (Dansgaard, 1964; Rozanski et al., 1993; Vuille et al., 2003; Fairchild et al., 2006). Noteworthy, neither Cariaco Ti nor gray-scale records resemble the variability in terms of frequency and amplitude observed over the time windows covered by our stable isotope $\delta^{18}O$ records, suggesting that rainfall is not the sole control of the amount of detrital material delivered to Cariaco (Martinez et al., 2007).

Between 8.0 and 6.5 ka BP, the enhancement of the annual cycle likely led to mostly wet and in-phase conditions between Venezuela and Cuba (Fensterer et al., 2013). Between 6.0 and 5.0 ka, dry conditions are observed in the Caribbean, which is attributed to an increase in iceberg discharge to both the cold polar East Greenland Current (EGC) and the subpolar warm North Atlantic Drift (NAD) and a reduction of NADW formation (Bond et al., 2001; Oppo et al., 2003; Moros et al., 2006), leading to severe cold, winter-like atmospheric conditions (O'Brien et al., 1995; Oppo et al., 2003; Jackson et al., 2005), a southward NASH position (Sullivan et al., 2021) and the highest north-central Venezuela (VEAJ) $\delta^{18}O$ values, peaking around 5.2 ka. This period likely represents the southernmost position attained by the ITCZ during the mid-Holocene, which might have contributed to wetter conditions in the SAMS domain.

In contrast to the mid-Holocene, hydroclimate variability in northeastern Venezuela (VECA) varies in phase with the SH records during the last 1000 years, with the AMO (Mann et al., 2009) affecting both regions in the same way. During the MCA, the ITCZ might have been located north of northern Venezuela, leading to drier conditions, especially during positive AMO phases when the ITCZ was likely displaced even farther to the north. During the first part of the LIA, the ITCZ might have been located over the equatorial latitudes, driving moisture influx to northeastern Venezuela (Curtis et al., 1999; Polissar et al., 2013), central Colombia (Bird et al., 2018) and the SAMS domain (Bird et al., 2011; Apaestegui et al., 2014; Della Libera et al., 2022). No speleothem deposition occurred during the main LIA period, which might be related to drier conditions in response to a southward displacement of the ITCZ. The CWP is characterized by a trend toward increased precipitation in northeastern Venezuela, contrasting the trend toward dryer conditions observed in the SAMS records (Bird et al., 2011; Vuille et al., 2012), and supporting the TraCE-21 ka simulations showing a NH-SH monsoons asymmetry induced by the non-uniform warming induced by the larger NH continental area (He et al., 2022).

Author contributions

I declare, all authors made substantial contributions to the present manuscript and have approved the final version: N. Melissa M. Medina: conceptualization, formal analysis, investigation, methodology, visualization, writing- original draft, writing-review-editing. Francisco W. Cruz: conceptualization, formal analysis, resources, funding acquisition, project administration, supervision, visualization, writing-review-editing. Amos Winter: resources, formal analysis, supervision, writing-review-editing. Haiwei Zhang: formal analysis, resources, methodology, writing-review-editing. Angela Ampuero: formal analysis, visualization, methodology, writing-review-editing. Mathias Vuille: formal analysis, writing-review-editing, validation. Victor C. Mayta: formal analysis, visualization, methodology, writing-review-editing. Marília C. Campos: formal analysis, investigation, writing-review-editing,

validation. Veronica M. Ramirez: formal analysis, review, methodology. Giselle Utida: formal analysis, review, methodology. Andres C. Zúñiga: formal analysis, review, methodology, Hai Cheng: resources, funding acquisition, project administration.

Declaration of competing interest

The authors declare that they have no known competing financial interests or personal relationships that could have appeared to influence the work reported in this paper.

Data availability

The new records from Alfredo Jahn and Caripe caves will be available at PANGEA.

Acknowledgments

We thank the São Paulo Research Foundation (FAPESP) and National Science Foundation (NSF-PIRE) award for financial support through FAPESP Pire Project 2017/50085e3 to FWC, NSF-PIRE grant OISE-1743738 to MV, FAPESP fellowship 2019/16745-1 grant to NMMM and grant 2019/25179e0 for MCC. We are also grateful with Franco Urbani, Rafael Carreño, Luz María Rodriguez and Govinda Galindo from Sociedad Venezolana de Espeleología (SVE) for their assistance during the field trip. We thank Sergio Foghin from the Universidad Pedagogica Experimental Libertador (Venezuela) for providing us meteorological data from the INAMEH and Maria Souza for her assistance in the laboratory. We also acknowledge the thoughtful comments from two anonymous reviewers that greatly improved the manuscript.

Appendix A. Supplementary data

Supplementary data to this article can be found online at https://doi.org/10.1016/j.quascirev.2023.108056.

References

Apaestegui, J., Cruz, F.W., Sifeddine, A., Vuille, M., Espinoza, J.C., Guyot, J.L., Khodri, M., Strikis, N., Santos, R.V., Cheng, H., Edwards, L., Carvalho, E., Santini, W., 2014. Hydroclimate variability of the northwestern Amazon Basin near the Andean foothills of Peru related to the South American Monsoon System during the last 1600 years. Clim. Past 10 (6), 1967e1981. https://doi.org/10.5194/cp-10-1967-2014.

Berger, A., Loutre, M.F., 1991. Insolation values for the climate of the last 10 million years. Quat. Sci. Rev. 10 (4), 297e317. https://doi.org/10.1016/0277-3791(91)90033-Q.

Bird, B.W., Abbott, M.B., Vuille, M., Rodbell, D.T., Stansell, N.D., Rosenmeier, M.F., 2011. A 2,300-year-long annually resolved record of the South American summer monsoon from the Peruvian Andes. Proc. Natl. Acad. Sci. U.S.A. 108 (21), 8583e8588. https://doi.org/10.1073/pnas.1003719108.

Bird, B.W., Rudloff, O., Escobar, J., Gilhooly, W.P., Correa-Metrio, A., Velez, M., Polissar, P.J., 2018. Paleoclimate support for a persistent dry island effect in the Colombian Andes during the last 4700 years. Holocene 28 (2), 217e228. https://doi.org/10.1177/0959683617721324.

Black, D.E., Peterson, L.C., Overpeck, J.T., Kaplan, A., Evans, M.N., Kashgarian, M., 1999. Eight centuries of North Atlantic ocean atmosphere variabitity. Science 286 (5445), 1709e1713. https://doi.org/10.1126/science.286.5445.1709.

Bohm, E., Lippold, J., Gutjahr, M., Frank, M., Blaser, P., Antz, B., Fohlmeister, J., Frank, N., Andersen, M.B., Deininger, M., 2015. Strong and deep Atlantic meridional overturning circulation during the last glacial cycle. Nature 517 (7532), 73e76. https://doi.org/10.1038/nature14059.

Bond, G., Kromer, B., Beer, J., Muscheler, R., Evans, M.N., Showers, W., Hoffmann, S., Lotti-Bond, R., Hajdas, I., Bonani, G., 2001. Persistent solar influence on North Atlantic climate during the Holocene. Science 294 (5549), 2130e2136. https://doi.org/10.1126/science.1065680.

Bradbury, J.P., Leyden, B., Salgado-Labouriau, M., Lewis, W.M., Schubert, J.C., Binford, M.W., Frey, D.G., Whitehead, D.R., Weibezahn, F.H., 1981. Late quaternary environmental history of lake Valencia, Venezuela. Science 214 (4527).

Bustamante, M.G., Cruz, F.W., Vuille, M., Apaestegui, J., Strikis, N., Panizo, G., Novello, F.V., Deininger, M., Sifeddine, A., Cheng, H., Moquet, J.S., Guyot, J.L., Santos, R.V., Segura, H., Edwards, R.L., 2016. Holocene changes in monsoon precipitation in the Andes of NE Peru based on $\delta^{18}O$ speleothem records. Quat. Sci. Rev. 146, 274e287. https://doi.org/10.1016/j.quascirev.2016.05.023.

Campos, M.C., Chiessi, C.M., Novello, V.F., Crivellari, S., Campos, J.L.P.S., Albuquerque, A.L.S., Venancio, I.M., Santos, T.P., Melo, D.B., Cruz, F.W., Sawakuchi, A.O., Mendes, V.R., 2022. South American precipitation dipole forced by interhemispheric temperature gradient. Sci. Rep. 12 (1), 1e9. https://doi.org/10.1038/s41598-022-14495-1.

Cheng, H., Fleitmann, D., Edwards, R.L., Wang, X., Cruz, F.W., Auler, A.S., Mangini, A., Wang, Y., Kong, X., Burns, S.J., Matter, A., 2009. Timing and structure of the 8.2. kyr B.P. event inferred from d 18O records of stalagmites from China, Oman, and Brazil. Geology 37 (11), 1007e1010. https://doi.org/10.1130/G30126A.1.

Cheng, H., Lawrence Edwards, R., Shen, C.C., Polyak, V.J., Asmerom, Y., Woodhead, J., Hellstrom, J., Wang, Y., Kong, X., Spötl, C., Wang, X., Calvin Alexander, E., 2013. Improvements in 230Th dating, 230Th and 234U half-life values, and U-Th isotopic measurements by multi-collector inductively coupled plasma mass spectrometry. Earth Planet. Sci. Lett. 371e372, 82e91. https://doi.org/10.1016/j.epsl.2013.04.006.

Chiang, J.C.H., Bitz, C.M., 2005. Influence of high latitude ice cover on the marine Intertropical Convergence Zone. Clim. Dynamics 25 (5), 477e496. https://doi.org/10.1007/s00382-005-0040-5.

Chiessi, C.M., Mulitza, S., Taniguchi, N.K., Prange, M., Campos, M.C., Häggi, C., Schefuß, E., Pinho, T.M.L., Frederichs, T., Portilho-Ramos, R.C., Sousa, S.H.M., Crivellari, S., Cruz, F.W., 2021. Mid- to late Holocene contraction of the intertropical convergence Zone over northeastern South America. Paleoceanogr. Paleoclimatol. 36 (4), 1e20. https://doi.org/10.1029/2020PA003936.

Clement, A.C., Seager, R., Cane, M.A., 1999. Orbital controls on the El niño/southern oscillation and the tropical climate. Paleoceanography 14 (4), 441e456. https://doi.org/10.1029/1999PA900013.

Coe, M.T., Bonan, G.B., 1997. Feedbacks between climate and surface water in northern Africa during the middle Holocene. J. Geophys. Res. 102, 11087e11101.

Conroy, J.L., Restrepo, A., Overpeck, J.T., Steinitz-Kannan, M., Cole, J.E., Bush, M.B., Colinvaux, P.A., 2009. Unprecedented recent warming of surface temperatures in the eastern tropical Pacific Ocean. Nat. Geosci. 2 (1), 46e50. https://doi.org/10.1038/ngeo390.

Cruz, F.W., Vuille, M., Burns, S.J., Wang, X., Cheng, H., Werner, M., Edwards, R.L., Karmann, I., Auler, A.S., Nguyen, H., 2009. Orbitally driven east-west antiphasing of South American precipitation. Nat. Geosci. 2 (3), 210e214. https://doi.org/10.1038/ngeo444.

Curtis, J.H., Brenner, M., Hodell, D.A., 1999. Climate change in the Lake Valencia basin, Venezuela, ~12600 yr BP to present. Holocene 9 (5), 609e619. https://doi.org/10.1191/095968399669724431.

Dansgaard, W., 1964. Stable isotopes in precipitation. Tellus 16 (4), 436e468. https://doi.org/10.3402/tellusa.v16i4.8993.

Della Libera, M.E., Novello, V.F., Cruz, F.W., Orrison, R., Vuille, M., Maezumi, S.Y., de Souza, J., Cauhy, J., Campos, J.L.P.S., Ampuero, A., Utida, G., Strikis, N.M., Stumpf, C.F., Azevedo, V., Zhang, H., Edwards, R.L., Cheng, H., 2022. Paleoclimatic and paleoenvironmental changes in Amazonian lowlands over the last three millennia. Quat. Sci. Rev. 279. https://doi.org/10.1016/j.quascirev.2022.107383.

Deplazes, G., Lückge, A., Peterson, L.C., Timmermann, A., Hamann, Y., Hughen, K.A., Röhl, U., Laj, C., Cane, M.A., Sigman, D.M., Haug, G.H., 2013. Links between tropical rainfall and North Atlantic climate during the last glacial period. Nat. Geosci. 6 (3), 213e217. https://doi.org/10.1038/ngeo1712.

Dykoski, C.A., Edwards, R.L., Cheng, H., Yuan, D., Cai, Y., Zhang, M., Lin, Y., Qing, J., An, Z., Revenaugh, J., 2005. A high-resolution, absolute-dated Holocene and deglacial Asian monsoon record from Dongge Cave, China. Earth Planet Sci. Lett. 233 (1e2), 71e86. https://doi.org/10.1016/j.epsl.2005.01.036.

Fairchild, I.J., Smith, C.L., Baker, A., Fuller, L., Spötl, C., Mattey, D., McDermott, F., 2006. Modification and preservation of environmental signals in speleothems. Earth Sci. Rev. 75 (1e4), 105e153. https://doi.org/10.1016/j.earscirev.2005.08.003.

Fensterer, C., Scholz, D., Hoffmann, D.L., Spötl, C., Schröder-Ritzrau, A., Horn, C., Pajon, J.M., Mangini, A., 2013. Millennial-scale climate variability during the last 12.5ka recorded in a Caribbean speleothem. Earth Planet Sci. Lett. 361, 143e151. https://doi.org/10.1016/j.epsl.2012.11.019.

Fensterer, C., Scholz, D., Hoffmann, D., Spötl, C., Pajon, J.M., Mangini, A., 2012. Cuban stalagmite suggests relationship between Caribbean precipitation and the Atlantic Multidecadal Oscillation during the past 1 . 3 ka. Holocene 22 (12), 1405e1412. https://doi.org/10.1177/0959683612449759.

Forti, P., Urbani, F., Rossi, A., 1999. Minerales secundarios de las Cuevas del Indio y Alfredo Jahn, Estado Miranda, Venezuela. In: Boletín Informativo de La Comision de Geoespeleología (Federacion Espeleologica de America Latina y El Caribe -FEALC-), 7, pp. 1e6.

Fröhlich, K., Gibson, J.J., Aggarwal, P.K., 2002. Proceedings of the Study of Environmental Change Using Isotope Techniques. In: Deuterium Excess in Precipitation and its Climatological Significance. International Atomic Energy Agency, IAEA-CSP, pp. 54e66.

Gibson, K.A., Peterson, L.C., 2014. A 0.6 million year record of millennial-scale variability in the tropics. Geophys. Res. Lett. 41, 969e975. https://doi.org/10.1002/2013GL058846.

Goni, M.A., Woodworth, M.P., Aceves, H.L., Thunell, R.C., Tappa, E., Black, D., Müller-Karger, F., Astor, Y., Varela, R., 2004. Generation, transport, and preservation of the alkenone-based $U^{K}_{37}0$ sea surface temperature index in the water column and sediments of the Cariaco Basin (Venezuela). Global Biogeochem. Cycles 18 (2), 1e21. https://doi.org/10.1029/2003GB002132.

Gonzalez, C., Dupont, L.M., Behling, H., Wefer, G., 2008. Neotropical vegetation response to rapid climate changes during the last glacial period: palynological evidence from the Cariaco Basin. Quat. Res. 69 (2), 217e230. https://doi.org/10.1016/j.yqres.2007.12.001.

Hastenrath, S., 1984. Interannual variability and annual cycle: mechanisms of circulation and climate in the tropical atlantic sector. Mon. Weather Rev. 112, 1097e1107.

Haug, G.H., Hughen, K.A., Sigman, D.M., Peterson, L.C., Ro, U., 2001. Southward migration of the intertropical convergence Zone through the Holocene. Science 293 (5533), 1304e1309. https://doi.org/10.1126/science.1059725.

He, P., Liu, J., Wang, B., Sun, W., 2022. Understanding global monsoon precipitation changes during the 8.2 ka event and the current warm period. Palaeogeogr. Palaeoclimatol. Palaeoecol. 586 (110757), 1e13. https://doi.org/10.1016/j.palaeo.2021.110757.

Herbert, T.D., Schuffert, J.D., 2000. Alkenone unsaturation estimates of sea-surface temperatures at Site 1002 over a full glacial cycle. In: Proceedings of the Ocean Drilling Program: Scientific Results, 165, pp. 239e247. https://doi.org/10.2973/odp.proc.sr.165.030.2000 (June).

Hodell, D.A., Brenner, M., Curtis, J.H., Medina-Gonzalez, R., Ildefonso-Chan Can, E., Albornaz-Pat, A., Guilderson, T.P., 2005. Climate change on the yucatan peninsula during the little ice age. Quat. Res. 63 (2), 109e121. https://doi.org/10.1016/j.yqres.2004.11.004.

Hodell, D.A., Curtis, J.H., Jones, G.A., Higuera-Gundy, A., Brenner, M., Binford, M.W., Dorsey, K.T., 1991. Reconstruction of Caribbean climate change over the past 10,500 years. Nature 352, 790e793. https://doi.org/10.1038/255242a0.

Huffman, G.J., Stocker, D.T., Bolvin, E.J., Nelkin, J., 2019. GPM IMERG final precipitation L3 1 day 0.1 degree x 0.1 degree (No. V06). In: Savtchenko, Andrey, Greenbelt, M.D. (Eds.), Goddard Earth Sciences Data and Information Services Center (GES DISC).

Hughen, K.A., Southon, J.R., Lehman, S.J., Overpeck, J.T., 2000. Synchronous radiocarbon and climate shifts during the last deglaciation. Science 290 (5498), 1951e1954. https://doi.org/10.1126/science.290.5498.1951.

Hughen, K.A., Overpeck, J.T., Peterson, L.C., Anderson, R.F., 1996. The nature of varved sedimentation in the Cariaco Basin, Venezuela, and its palaeoclimatic significance. Geol. Soc. Spec. Publ. 116 (116), 171e183. https://doi.org/10.1144/GSL.SP.1996.116.01.15.

Jackson, M.G., Oskarsson, N., Trønnes, R.G., McManus, J.F., Oppo, D.W., Gr€onvold, K., Hart, S.R., Sachs, J.P., 2005. Holocene loess deposition in Iceland: evidence for millennial-scale atmosphere-ocean coupling in the North Atlantic. Geology 33 (6), 509e512. https://doi.org/10.1130/G21489.1.

Jin, C., Wang, B., Liu, J., 2020. Future changes and controlling factors of the eight regional monsoons projected by CMIP6 models. J. Clim. 33 (21), 9307e9326. https://doi.org/10.1175/JCLI-D-20-0236.1.

Kanner, L.C., Burns, S.J., Cheng, H., Edwards, R.L., Vuille, M., 2013. High-resolution variability of the South American summer monsoon over the last seven millennia: Insights from a speleothem record from the central Peruvian Andes. Quat. Sci. Rev. 75, 1e10. https://doi.org/10.1016/j.quascirev.2013.05.008.

Lachniet, M.S., Asmerom, Y., Burns, S.J., Patterson, W.P., Polyak, V.J., Seltzer, G.O., 2004. Tropical response to the 8200 yr B.P cold event? Speleothem isotopes indicate a weakened early Holocene monsoon in Costa Rica. Geology 32 (11), 957e960. https://doi.org/10.1130/G20797.1.

Lane, C.S., Horn, S.P., Orvis, K.H., Thomason, J.M., 2011. Oxygen isotope evidence of little ice age aridity on the caribbean slope of the Cordillera central, Dominican republic. Quat. Res. 75 (3), 461e470. https://doi.org/10.1016/j.yqres.2011.01.002.

Lea, D.W., Pak, D.K., Peterson, L.C., Hughen, K.A., 2003. Synchroneity of tropical and high-latitude Atlantic temperatures over the last glacial termination. Science 301 (5638), 1361e1364. https://doi.org/10.1126/science.1088470.

Ledru, M.P., 2001. Late Holocene rainforest disturbance in French Guiana. Rev. Palaeobot. Palynol. 115 (3e4), 161e170. https://doi.org/10.1016/S0034-6667(01)00068-9.

Liu, F., Wang, B., Ouyang, Y., Wang, H., Qiao, S., Chen, G., Dong, W., 2022. Intraseasonal variability of global land monsoon precipitation and its recent trend. Npj Climate and Atmospheric Science 5 (1). https://doi.org/10.1038/s41612-022-00253-7.

Mangini, A., Blumbach, P., Verdes, P., Sp€ol, C., Scholz, D., Machel, H., Mahon, S., 2007. Combined records from a stalagmite from Barbados and from lake sediments in Haiti reveal variable seasonality in the Caribbean between 6.7 and 3 ka BP. Quat. Sci. Rev. 26 (9e10), 1332e1343. https://doi.org/10.1016/j.quascirev.2007.01.011.

Mann, M.E., Zhang, Z., Rutherford, S., Bradley, R.S., Hughes, M.K., Shindell, D., Ammann, C., Faluvegi, G., Fenbiao, N., 2009. Global signatures and dynamical origins of the little ice age and medieval climate anomaly. Science 326, 1256e1260.

Marcott, S.A., Clark, P.U., Padman, L., Klinkhammer, G.P., Springer, S.R., Liu, Z., Otto-Bliesner, B.L., Carlson, A.E., Ungerer, A., Padman, J., He, F., Cheng, J., Schmittner, A., 2011. Ice-shelf collapse from subsurface warming as a trigger for Heinrich events. Proc. Natl. Acad. Sci. U.S.A. 108 (33), 13415e13419. https://doi.org/10.1073/pnas.1104772108.

Martinez, C., Goddard, L., Kushnir, Y., Ting, M., 2019. Seasonal climatology and dynamical mechanisms of rainfall in the Caribbean. Clim. Dynam. 53 (1e2), 825e846. https://doi.org/10.1007/s00382-019-04616-4.

Martinez, N.C., Murray, R.W., Thunell, R.C., Peterson, L.C., Muller-Karger, F., Astor, Y., Varela, R., 2007. Modern climate forcing of terrigenous deposition in the tropics (Cariaco Basin, Venezuela). Earth Planet Sci. Lett. 264 (3e4), 438e451. https://doi.org/10.1016/j.epsl.2007.10.002.

McGee, D., Donohoe, A., Marshall, J., Ferreira, D., 2014. Changes in ITCZ location and cross-equatorial heat transport at the last glacial maximum, Heinrich stadial 1, and the mid-holocene. Earth Planet Sci. Lett. 390, 69e79. https://doi.org/10.1016/j.epsl.2013.12.043.

Moberg, A., Sonechkin, D.M., Holmgren, K., Datsenko, M.H., Karlen, W., 2005. Highly variable Northern Hemisphere temperatures reconstructed from low- and high-resolution proxy data. Nature 433 (7026), 613e617. https://doi.org/10.1038/nature03265.

Moros, M., Andrews, J.T., Eberl, D.D., Jansen, E., 2006. Holocene history of drift ice in the northern North Atlantic: evidence for different spatial and temporal modes. Paleoceanography 21 (2), 1e10. https://doi.org/10.1029/2005PA001214.

Moy, C.M., Seltzer, G.O., Rodbell, D.T., Anderson, D.M., 2002. Variability of El niño/southern oscillation activity at millennial timescales during the Holocene epoch. Nature 420 (6912), 162e165. https://doi.org/10.1038/nature01194.

Mulitza, S., Chiessi, C.M., Schefuß, E., Lippold, J., Wichmann, D., Antz, B., Mackensen, A., Paul, A., Prange, M., Rehfeld, K., Werner, M., Bickert, T., Frank, N., Kuhnert, H., Lynch-Stieglitz, J., Portilho-Ramos, R.C., Sawakuchi, A.O., Schulz, M., Schwenk, T., et al., 2017. Synchronous and proportional deglacial changes in Atlantic meridional overturning and northeast Brazilian precipitation. Paleoceanography 32 (6), 622e633. https://doi.org/10.1002/2017PA003084.

Novello, V.F., Cruz, F.W., Moquet, J.S., Vuille, M., de Paula, M.S., Nunes, D., Edwards, R.L., Cheng, H., Karmann, I., Utida, G., Stríkis, N.M., Campos, J.L.P.S., 2018. Two millennia of south atlantic convergence Zone variability reconstructed from isotopic proxies. Geophys. Res. Lett. 45 (10), 5045e5051. https://doi.org/10.1029/2017GL076838.

Novello, V.F., Cruz, F.W., Karmann, I., Burns, S.J., Stríkis, N.M., Vuille, M., Cheng, H., Edwards, R.L., Santos, R.V., Frigo, E., Barreto, E.A.S., 2012. Multidecadal climate variability in Brazil's Nordeste during the last 3000 years based on speleothem isotope records. Geophys. Res. Lett. 39 (23), 1e6. https://doi.org/10.1029/2012GL053936.

O'Brien, S.R., Mayewski, P.A., Meeker, L.D., Meese, D.A., Twickler, M.S., Whitlow, S., 1995. Complexity of Holocene climate as reconstructed from a Greenland ice core. Science 270 (21), 1962e1964. https://doi.org/10.1126/science.270.5244.1962.

Oppo, D.W., McManus, J.F., Cullen, J.L., 2003. Deepwater variability in the Holocene epoch. Nature 422 (6929), 277. https://doi.org/10.1038/422277b, 277.

Peterson, L.C., Haug, G.H., Hughen, K.A., Rohl, U., 2000. Rapid changes in the hydrologic cycle of the tropical Atlantic during the last glacial. Science 290 (5498), 1947e1951. https://doi.org/10.1126/science.290.5498.1947.

Peterson, L.C., Overpeck, J.T., Kipp, N.G., Imbrie, J., 1991. A high-resolution Late Quaternary upwelling record from the anoxic Cariaco Basin, Venezuela. Paleoceanography 6 (1), 99e119. https://doi.org/10.1029/90PA02497.

Peterson, Larry C., Haug, G.H., 2006. Variability in the mean latitude of the atlantic intertropical convergence Zone as recorded by riverine input of sediments to the Cariaco Basin (Venezuela). Palaeogeogr. Palaeoclimatol. Palaeoecol. 234 (1), 97e113. https://doi.org/10.1016/j.palaeo.2005.10.021.

Polissar, P.J., Abbott, M.B., Wolfe, A.P., Bezada, M., Rull, V., Bradley, R.S., 2006. Solar modulation of little ice age climate in the tropical Andes. Proc. Natl. Acad. Sci. U.S.A. 103 (24), 8937e8942. https://doi.org/10.1073/pnas.0603118103.

Polissar, P.J., Abbott, M.B., Wolfe, A.P., Vuille, M., Bezada, M., 2013. Synchronous interhemispheric Holocene climate trends in the tropical Andes. Proc. Natl. Acad. Sci. U.S.A. 110 (36), 14551e14556. https://doi.org/10.1073/pnas.1219681110.

Poveda, G., Waylen, P.R., Pulwarty, R.S., 2006. Annual and inter-annual variability of the present climate in northern South America and southern Mesoamerica. Palaeogeogr. Palaeoclimatol. Palaeoecol. 234 (1), 3e27. https://doi.org/10.1016/j.palaeo.2005.10.031.

Pulwarty, R.S., Barry, R.G., Riehl, H., 1992. Annual and Seasonal Patterns of Rainfall Variability over Venezuela (Jährliche und jahreszeitliche Muster der Niederschlagsvariabilität in Venezuela). Erdkunde 46 (3/4), 273e289.

Reuter, J., Stott, L., Khider, D., Sinha, A., Cheng, H., Edwards, R.L., 2009. A new perspective on the hydroclimate variability in northern South America during the Little Ice Age. Geophys. Res. Lett. 36 (21), 1e5. https://doi.org/10.1029/2009GL041051.

Rozanski, K., Araguas-Araguas, L., Gonfiantini, R., 1993. Isotopic patterns in modern global precipitation. Climate Change in Continental Isotopic Records: American Geophysical Union Geophysical Monograph 78, 1e36. https://doi.org/10.1029/gm078p0001.

Rozanski, K., Sonntag, C., Munnich, K., 1982. Factors controlling stable isotope composition of European precipitation. Tellus 34, 142e150.

Scholz, D., Hoffmann, D.L., 2011. StalAge - an algorithm designed for construction of speleothem age models. Quat. Geochronol. 6 (3e4), 369e382. https://doi.org/10.1016/j.quageo.2011.02.002.

Stríkis, N.M., Chiessi, C.M., Cruz, F.W., Vuille, M., Cheng, H., De Souza Barreto, E.A., Mollenhauer, G., Kasten, S., Karmann, I., Edwards, R.L., Bernal, J.P., Sales, H.D.R., 2015. Timing and structure of mega-SACZ events during Heinrich stadial 1. Geophys. Res. Lett. 42 (13), 5477e5484. https://doi.org/10.1002/2015GL064048.

Stríkis, N.M., Cruz, F.W., Cheng, H., Karmann, I., Edwards, R.L., Vuille, M., Wang, X., de Paula, Novello, V.F., Auler, A.S., 2011. Abrupt variations in South American monsoon rainfall during the Holocene based on a speleothem record from central-eastern Brazil. Geology 39 (11), 1075e1078. https://doi.org/10.1130/G32098.1.

Sullivan, R.M., van Hengstum, P.J., Coats, S.J., Donnelly, J.P., Tamalavage, A.E., Winkler, T.S., Albury, N.A., 2021. Hydroclimate dipole drives multi-centennial variability in the western tropical North Atlantic margin during the middle

and late Holocene. Paleoceanogr. Paleoclimatol. 36 (7), 1e16. https://doi.org/10.1029/2020PA004184.

Urbani, F., 1973. Carsos de Venezuela, Parte 2: Calizas Metamorficas de la Cordillera de la Costa. Boletin de La Sociedad Venezolana de Espeleología 4 (1), 15e37.

Utida, G., Cruz, F.W., Santos, R.V., Sawakuchi, A.O., Wang, H., Pessenda, L.C.R., Novello, V.F., Vuille, M., Strauss, A.M., Borella, A.C., Stríkis, N.M., Guedes, C.C.F., Dias De Andrade, F.R., Zhang, H., Cheng, H., Edwards, R.L., 2020. Climate changes in Northeastern Brazil from deglacial to Meghalayan periods and related environmental impacts. Quat. Sci. Rev. 250. https://doi.org/10.1016/j.quascirev.2020.106655.

Vellinga, M., Wood, R.A., 2002. Global climatic impacts of a collapse of the atlantic thermohaline circulation. Clim. Change 54 (3), 251e267. https://doi.org/10.1023/A:1016168827653.

Vuille, M., Bradley, R.S., Werner, M., Healy, R., Keimig, F., 2003. Modeling $\delta^{18}O$ in precipitation over the tropical Americas: 1. Interannual variability and climatic controls. J. Geophys. Res. Atmos. 108 (6). https://doi.org/10.1029/2001jd002038.

Vuille, M., Burns, S.J., Taylor, B.L., Cruz, F.W., Bird, B.W., Abbott, M.B., Kanner, L.C., Cheng, H., Novello, V.F., 2012. A review of the South American monsoon history as recorded in stable isotopic proxies over the past two millennia. Clim. Past 8 (4), 1309e1321. https://doi.org/10.5194/cp-8-1309-2012.

Winter, A., Miller, T., Kushnir, Y., Sinha, A., Timmermann, A., Jury, M.R., Gallup, C., Cheng, H., Edwards, R.L., 2011. Evidence for 800 years of North Atlantic multi-decadal variability from a Puerto Rican speleothem. Earth Planet Sci. Lett. 308 (1e2), 23e28. https://doi.org/10.1016/j.epsl.2011.05.028.

Wurtzel, J.B., Black, D.E., Thunell, R.C., Peterson, L.C., Tappa, E.J., Rahman, S., 2013. Mechanisms of southern Caribbean SST variability over the last two millennia. Geophys. Res. Lett. 40 (22), 5954e5958. https://doi.org/10.1002/2013GL058458.

Yarincik, K.M., Murray, R.W., Lyons, T.W., Peterson, L.C., Haug, G.H., 2000. Oxygenation history of bottom waters in the Cariaco Basin, Venezuela, over the past 578,000 years: results from redox-sensitive metals (Mo, V, Mn, and Fe). Paleoceanography 15 (6), 593e604. https://doi.org/10.1029/1999PA000401.